HHS Public Access

Author manuscript

Science. Author manuscript; available in PMC 2021 June 04.

Published in final edited form as:

Science. 2021 May 14; 372(6543): 716–721. doi:10.1126/science.aaz2740.

Cell-specific transcriptional control of mitochondrial metabolism by TIF1γ drives erythropoiesis

Marlies P. Rossmann[1,2], **Karen Hoi**[1,2], **Victoria Chan**[1,2], **Brian J. Abraham**[3,†], **Song Yang**[2], **James Mullahoo**[4], **Malvina Papanastasiou**[4], **Ying Wang**[5], **Ilaria Elia**[6], **Julie R. Perlin**[2], **Elliott J. Hagedorn**[2], **Sara Hetzel**[7], **Raha Weigert**[7], **Sejal Vyas**[6], **Partha P. Nag**[4], **Lucas B. Sullivan**[8], **Curtis R. Warren**[9,‡], **Bilguujin Dorjsuren**[1,2], **Eugenia Custo Greig**[1,2], **Isaac Adatto**[1,2], **Chad A. Cowan**[9], **Stuart L. Schreiber**[4], **Richard A. Young**[3,10], **Alexander Meissner**[1,4,7], **Marcia C. Haigis**[6], **Siegfried Hekimi**[5], **Steven A. Carr**[4], **Leonard I. Zon**[1,2,*]

[1]Department of Stem Cell and Regenerative Biology, Harvard University, Cambridge, MA 01238, USA.

[2]Stem Cell Program and Division of Hematology/Oncology, Boston Children's Hospital and Dana-Farber Cancer Institute, Howard Hughes Medical Institute, Harvard Stem Cell Institute, Harvard Medical School, Boston, MA 02115, USA.

[3]Whitehead Institute for Biomedical Research, Cambridge, MA 02142, USA.

[4]Broad Institute of MIT and Harvard, Cambridge, MA 02142, USA.

[*]Corresponding author. leonard.zon@enders.tch.harvard.edu.

[†]Present address: Department of Computational Biology, St. Jude Children's Research Hospital, Memphis, TN 38105, USA.

[‡]Present address: Cardiometabolic Disease Research, Boehringer-Ingelheim Pharmaceuticals Inc., Ridgefield, CT 06877, USA.

Author contributions: M.P.R. and L.I.Z. conceived the project; M.P.R. performed most of the experiments and analyzed the data. B.J.A. and S.Y. analyzed ChIP-seq and RNA-seq data. J.M., M.P., and S.A.C. performed histone modification analyses. Y.W. performed the CoQ measurements. I.E., S.V., and M.C.H. helped with metabolomics experiments. J.R.P. and E.J.H. helped with blastula transplantation experiments and imaging. S.H., R.W., and A.M. performed DNA methylation analyses. K.H., V.C., B.D., and E.C.G. provided research assistance. P.P.N. and S.L.S. provided synthetic chemistry and chemical biology expertise. L.B.S. provided constructive suggestions and protocols. C.R.W. and C.A.C. provided the Seahorse and expertise. I.A. provided zebrafish husbandry expertise. R.A.Y. provided feedback on study design and experimental results. M.P.R. and L.I.Z. wrote the manuscript with input from B.J.A., S.Y., J.M., M.P., I.E., J.R.P., E.J.H., S.H., R.W., P.P.N., L.B.S., C.R.W., E.C.G., S.L.S., R.A.Y., A.M., M.C.H., and S.H.

Competing interests: B.J.A. is a shareholder in Syros Pharmaceuticals. C.A.C. is a founder and Chief Scientific Officer of Sana Biotechnology. S.L.S. serves on the Board of Directors of the Genomics Institute of the Novartis Research Foundation (GNF), is a shareholder in and serves on the Board of Directors of Jnana Therapeutics, is a shareholder in Forma Therapeutics, is a shareholder in and advises Decibel Therapeutics and Eikonizo Therapeutics, serves on the Scientific Advisory Boards of Eisai Co., Ltd., Ono Pharma Foundation, Exo Therapeutics and F-Prime Capital Partners, and is a Novartis Faculty Scholar. R.A.Y. is a founder of and shareholder in Syros Pharmaceuticals, Camp4 Therapeutics, Omega Therapeutics and Dewpoint Therapeutics. M.C.H. serves on the Scientific Advisory Board of Pori Therapeutics. S.A.C. is a member of the scientific advisory boards of Kymera, PTM BioLabs and Seer, and is a scientific adviser to Pfizer and Biogen. L.I.Z. is a founder of and holds stock in Fate Therapeutics, Camp4 Therapeutics and Scholar Rock, and is a consultant to Celularity. All other authors declare no competing interests.

Data and materials availability: The RNA-seq, ChIP-seq, and RRBS data of this study are deposited in the NCBI Gene Expression Omnibus (GEO) under accession number GSE136456.

SUPPLEMENTARY MATERIALS

science.sciencemag.org/content/372/6543/716/suppl/DC1

Materials and Methods

Supplementary Text

Figs. S1 to S21

Table S1

References (*34*–*75*)

Data S1 to S4

MDAR Reproducibility Checklist

View/request a protocol for this paper from Bio-protocol.

[5]Department of Biology, McGill University, Montréal, Québec H3A 1B1, Canada.

[6]Department of Cell Biology, Blavatnik Institute, Harvard Medical School, Boston, MA 02115, USA.

[7]Department of Genome Regulation, Max Planck Institute for Molecular Genetics, 14195 Berlin, Germany.

[8]Human Biology Division, Fred Hutchinson Cancer Research Center, Seattle, WA 98109, USA.

[9]Beth Israel Deaconess Medical Center, Harvard Medical School, Boston, MA 02215, USA.

[10]Department of Biology, Massachusetts Institute of Technology, Cambridge, MA 02139, USA.

Abstract

Transcription and metabolism both influence cell function, but dedicated transcriptional control of metabolic pathways that regulate cell fate has rarely been defined. We discovered, using a chemical suppressor screen, that inhibition of the pyrimidine biosynthesis enzyme dihydroorotate dehydrogenase (DHODH) rescues erythroid differentiation in bloodless zebrafish *moonshine (mon)* mutant embryos defective for transcriptional intermediary factor 1 gamma (*tif1γ*). This rescue depends on the functional link of DHODH to mitochondrial respiration. The transcription elongation factor TIF1γ directly controls coenzyme Q (CoQ) synthesis gene expression. Upon *tif1γ* loss, CoQ levels are reduced, and a high succinate/α-ketoglutarate ratio leads to increased histone methylation. A CoQ analog rescues *mon*'s bloodless phenotype. These results demonstrate that mitochondrial metabolism is a key output of a lineage transcription factor that drives cell fate decisions in the early blood lineage.

Vertebrate embryos produce circulating red blood cells (RBCs) that are required for oxygen and carbon dioxide transport (1). During embryonic development, three overlapping hematopoietic waves can be distinguished that all produce RBCs (2). In mammals, primitive erythroblasts that emerge in the blood islands within the extraembryonic yolk sac give rise to primitive erythrocytes of the first transient wave, and a second wave generates definitive erythroid-myeloid progenitors in the hemogenic endothelium of the yolk sac. Definitive erythrocytes of the third wave arise from multipotent hematopoietic stem cells that are born in the aortic endothelium of the aorta-gonad-mesonephros region and sustain hematopoiesis throughout the lifetime of the animal. Primitive erythrocytes supply the embryo with the oxygen needed for its rapid proliferation. Failure to initiate the first wave of erythropoiesis leads to embryonic lethality (3). Erythroid lineage differentiation is regulated by key transcription factors (4), but the cellular mechanisms that allow the generation and differentiation of the first erythroid progenitors remain largely unknown. Stem and descendent progenitor cells differ by their metabolic profiles (5), but there is little in vivo evidence for a link between transcriptional regulation and metabolic changes during cell fate decisions.

DHODH inhibitors rescue defective *tif1γ*-dependent erythropoiesis

TIF1γ is essential for erythropoiesis from zebrafish to humans (6–10). Zebrafish *moonshine* (*mon*) mutant embryos defective for *tif1γ* do not make RBCs because of a transcription

elongation block characterized by aberrantly paused RNA polymerase II (Pol II) (9–11). To uncover other factors required for *tif1γ*-dependent erythropoiesis, we performed a high-content chemical suppressor screen of 3120 compounds with known bioactivities to rescue erythropoiesis in the *mon* mutant. We incubated embryos with compounds from 5.3 hours post fertilization (hpf) until 22 hpf, the time of gastrulation and primitive erythropoiesis, and assayed embryonic *βe3 globin* expression using whole-mount in situ hybridization (WISH; Fig. 1A). This strategy identified the drug leflunomide as an inhibitor of dihydroorotate dehydrogenase (DHODH), the enzyme catalyzing the fourth step in the de novo pyrimidine biosynthesis pathway (12). Although *mon* embryos treated with leflunomide or its active metabolite, A771726 (13), showed increased *βe3 globin* expression, their wild-type and heterozygous siblings were blocked in erythroid differentiation (Fig. 1B and fig. S1, A and B). The fact that both leflunomide and A771726 rescued erythropoiesis in *mon* mutants ruled out an involvement of the aryl hydrocarbon receptor in this process, of which leflunomide has been described as an agonist (14). The structurally divergent DHODH inhibitor brequinar (15) similarly rescued the blood defect in *tif1γ*-depleted embryos, both at the level of *βe3 globin* expression (fig. S1C) and hemoglobin synthesis (Fig. 1C and fig. S1D), indicative of terminal erythropoiesis. In control embryos, DHODH inhibition led to a reduction in the number of hemoglobinized differentiated RBCs (Fig. 1C and fig. S1D). Modeling predicted the structures of zebrafish and human DHODH, including the binding pockets for A771726 and brequinar, to be highly conserved (fig. S2, A to C). These results demonstrate that inhibition of DHODH activity is required to rescue defective *tif1γ*-dependent erythropoiesis.

We performed time course studies to establish the developmental window during which DHODH is active in *mon* embryos. Treating embryos with leflunomide during gastrulation, but not later, was sufficient to rescue erythropoiesis in *mon* embryos (fig. S3). These results assign a critical early function for *tif1γ*, when specification of the erythroid lineage is initiated within mesoderm at the end of gastrulation. Blastula transplantation experiments showed a non-cell-autonomous role for *tif1γ* (fig. S4, A and B) in addition to its cell-autonomous role in erythropoiesis (fig. S4, C and D). During its development, mesoderm lies above the yolk sac, a metabolically active tissue that is a source of nutrients for the embryo proper and is analogous to the mammalian yolk sac and placenta (16, 17). A non-cell-autonomous role of *tif1γ* could suggest a more direct metabolic function in the early embryo.

tif1γ loss leads to TCA cycle changes, DNA and histone hypermethylation

Because DHODH is the only enzyme of the pyrimidine de novo synthesis pathway located in mitochondria (18), we investigated whether mitochondrial metabolism was altered in *mon* mutant embryos. RNA-sequencing (RNA-seq) experiments for *tif1γ*-depleted embryos at 10 hpf (fig. S5 and data S1) revealed that 77% (182 genes) of genes encoding proteins with mitochondrial function (19) [95% (20 genes) when considering genes that encode for subunits of the respiratory chain] were transcriptionally down-regulated upon *tif1γ* loss of function (Fig. 2A, middle and right). By contrast, only 55% (or 1986 genes) of nonmitochondrial genes were transcriptionally down-regulated (Fig. 2A, left). Furthermore, mitochondrial genes were more significantly down-regulated compared with

nonmitochondrial genes (fig. S6). These results indicate that mitochondrial gene expression specifically depends on *tif1γ*. DHODH inhibition did not alter the expression of p53 target genes (20), cell cycle genes, or genes involved in mitochondrial fission or fusion in *tif1γ*-depleted embryos (fig. S7, A and B; fig. S8; and data S2) but did promote differentiation processes including hematopoiesis specifically upon *tif1γ* loss, as shown by Metascape pathway analysis (fig. S9, A to D). Untargeted metabolomics analysis of *mon drl:EGFP* embryos at 22 hpf (Fig. 2B and fig. S10, A and B) or *tif1γ*-depleted embryos at 11 or 22 hpf (fig. S10, C and D) revealed reduced levels of several tricarboxylic acid (TCA) cycle metabolites, including citrate, its isomerization intermediate *cis*-aconitate, isocitrate, oxaloacetate, α-ketoglutarate (α-KG, also called 2-oxoglutarate), malate, and the TCA-cycle-related metabolite aspartate, suggesting a more general mitochondrial defect.

The activity of 2-oxoglutarate-dependent dioxygenases (OGGDs), which include DNA and histone demethylases, can be inhibited by an increased ratio of succinate, L-2-hydroxyglutarate (2HG), or fumarate to α-KG (21). Increased DNA and histone methylation levels have been observed after conditional knockout of mitochondrial complex III subunit Rieske iron-sulfur protein (encoded by UQCRFS1) in the hematopoietic system (22, 23), and a biallelic variant in UQCRFS1 in humans has been recently described to cause anemia (24). In-depth TCA cycle metabolic analyses revealed that the succinate/α-KG ratio was significantly increased in *tif1γ*-depleted embryos (Fig. 2C), and the 2HG/α-KG and fumarate/α-KG ratios were elevated (fig. S10E). To address whether histone and DNA methylation levels were altered upon *tif1γ* loss, we profiled global chromatin modifications in histones extracted from *tif1γ*-depleted embryos at 22 hpf using quantitative targeted mass spectrometry (fig. S11, A and B). The absence of *tif1γ* led to significantly increased levels of the methylated histone species H3K27me1, H3K27me2, and H3K27me3, H3K36me2 and H3K36me3, as well as H4K20me2 (Fig. 2D and fig. S12, A and B), modifications that are removed by OGGDs (25). The levels of histone acetylation, phosphorylation, and ubiquitination remained unchanged (fig. S12A). The expression of histone demethylases in *tif1γ* knockdown and *mon* does not account for the changes in methylation (data S3). We next evaluated DNA methylation, which can be reversed by OGGDs. Reduced representation bisulfite sequencing (RRBS) experiments revealed significant hypermethylation of background (genome excluding CpG islands) CpG dinucleotides (CpGs; fig. S13, A and B, and data S4), which represented 94% of all CpGs covered by RRBS with at least 10 reads (fig. S13C). Our results indicate that the altered mitochondrial TCA cycle activity in the absence of *tif1γ* leads to an increased succinate/α-KG ratio that in turn results in changes in the epigenome with higher histone and DNA methylation levels.

Mitochondrial function is impaired upon *tif1γ* loss

To investigate whether *tif1γ* loss compromises mitochondrial function, we performed a high-throughput single-embryo analysis of the oxygen consumption rate (OCR). Embryos depleted for *tif1γ* exhibited a functional decrease in oxidative aerobic metabolism at 14 hpf compared with control embryos, as demonstrated by a significant decrease in the OCR at baseline (Fig. 3A and fig. S14A). Although DHODH inhibition by leflunomide treatment of wild-type embryos led to a reduced OCR, *tif1γ* depletion did not result in a further reduction. To estimate the reserve respiratory capacity, we treated embryos with the

uncoupling agent carbonyl cyanide 4-(trifluoromethoxy)phenylhydrazone (FCCP), which abolishes the proton gradient and thus leads to an increase in oxygen consumption. Upon addition of FCCP, *tif1γ* depletion rescued the reduced OCR of DHODH-inhibited embryos (Fig. 3A and fig. S14B), showing that the function of DHODH in mitochondrial respiration is intimately linked to TIF1γ. In agreement with decreased baseline oxygen consumption of *tif1γ*-depleted embryos, we found that the ratio of oxidized to reduced nicotinamide adenine dinucleotides (NAD^+/NADH), which directly correlates with the OCR, was lowered in *mon* embryos (Fig. 3B). By comparison, embryos of the same age that were depleted for *gata1a*, the master transcription factor of the erythroid lineage and thus for RBCs (fig. S14C), showed an increased OCR over control-depleted embryos (fig. S14, D to F). *Gata1*$^-$ mouse embryonic stem cells give rise to an abnormal and highly proliferative blast population (26) that might exhibit high levels of mitochondrial respiration (22). These data show that mitochondrial respiration is required for blood formation and that *tif1γ* is required for normal mitochondrial function.

tif1γ drives erythropoiesis by affecting the electron transport chain

DHODH catalyzes the oxidation of dihydroorotate into orotate by transferring electrons to CoQ in the electron transport chain (ETC) (27). Thus, DHODH functionally links the production of pyrimidines with the mitochondrial respiratory chain (Fig. 4A). Uridine, which is converted through the salvage pathway into uridine monophosphate, can bypass the inhibition of de novo pyrimidine synthesis (fig. S15A). Although the erythroid differentiation block caused by DHODH inhibition in wild-type and heterozygous embryos could be partially reversed by the addition of uridine (fig. S15, B and C), the rescue of the *mon* blood defect by DHODH inhibition was not affected by uridine (Fig. 4B and fig. S15B), which could be caused by a “rewired metabolism” in *mon* mutants that may allow for more salvage pathway activity. To test whether the rescue of the *mon* blood defect by DHODH inhibition depends on DHODH’s impact on mitochondrial electron transport, we cotreated *mon* embryos with leflunomide and rotenone, an inhibitor of complex I of the ETC. Indeed, rotenone reversed the rescue of *mon*’s blood defect by leflunomide, whereas on its own it did not rescue blood in *mon* (Fig. 4C). The antioxidant *N*-acetyl-L-cysteine did not rescue the *mon* blood defect (fig. S16). These results demonstrate that DHODH inhibition rescues the blood defect in *mon* embryos through its link to the ETC.

TIF1γ directly regulates CoQ levels in erythropoiesis

In the inner mitochondrial membrane, electrons are transferred from complex I or II to complex III in a manner dependent on CoQ, an electron carrier that cycles between three redox states (28). DHODH competes with complexes I and II of the ETC for CoQ as an electron acceptor (Fig. 4A). CoQ consists of a benzoquinone ring head group joined to a polyisoprenoid side chain (29), which is synthesized by an enzyme encoded by PDSS1 and PDSS2 in humans and zebrafish. The head group subsequently is modified by several COQ enzymes (fig. S17). *COQ2* deficiency in humans leads to pancytopenia and anemia in infancy, and quinone deficiencies can be rescued by an exogeneous ubiquinone analog (30). To evaluate the role of TIF1γ in the CoQ biosynthesis pathway, we generated stable human HepG2 cell lines that expressed one of two different *TIF1γ* shRNAs (shTIF1γ) or control

shRNAs (shCtrl) under doxycycline control. We chose HepG2 cells as metabolically active cells akin to the yolk sac in the early zebrafish embryo. In these clonal cell lines, shTIF1γ-1 and shTIF1γ-2 induction specifically reduced *TIF1γ* expression by 98% and 50%, respectively, after 48 hours (Fig. 5A and fig. S18A), which correlated with reduced TIF1γ protein levels (fig. S18B). At this time point, we performed RNA-seq analysis, comparing both shTIF1γ with both shCtrl clones, in combination with chromatin immunoprecipitation-sequencing (ChIP-seq) analysis for TIF1γ chromatin occupancy, to identify differentially expressed genes that are also direct TIF1γ targets. Direct TIF1γ target genes frequently belonged to metabolic pathways (fig. S18C). In particular, several genes encoding CoQ pathway enzymes were significantly down-regulated upon shTIF1γ-1 and shTIF1γ-2 knockdown, including *PDSS1* by 88% and 35% and *COQ8A* by 42% and 69%, respectively, as well as *PDSS2* by 57% and *COQ2* by 84% in the more potent shTIF1γ-1 condition. Expression of the actin gene *ACTA2* remained unaffected by *TIF1γ* knockdown (fig. S18A). At the protein level, PDSS1 was down-regulated twofold upon *TIF1γ* knockdown (Fig. 5B). ChIP-seq analysis revealed that TIF1γ bound to the loci of these CoQ pathway genes and was often accompanied by the histone mark H3K27Ac, decorating active promoters and enhancers (Fig. 5C and fig. S19). These data establish that CoQ biosynthesis genes are direct targets of TIF1γ.

We hypothesized that down-regulation of CoQ pathway genes upon *TIF1γ* depletion and exhausted CoQ levels could be functionally relevant to the role of *tif1γ* in embryonic erythropoiesis. To test this idea, we measured CoQ levels in the zebrafish. We first determined that, as in humans but unlike in mice (28), the zebrafish CoQ isoprenoid side chain consists of 10 subunits (fig. S20A). Although the *mon* mutant is embryonically lethal, in rare cases, homozygous mutant *mon* fish survive into adulthood despite producing only very few mature RBCs (9). In other animals, livers have been described to contain normal levels of CoQ (31). In a large-scale effort, we generated sufficient numbers of *mon* fish, dissected their livers at 2 and 4.5 months, and found that CoQ_{10} levels were significantly reduced (Fig. 5D) and CoQ biosynthesis gene expression was down-regulated (fig. S20B and supplementary text). Treatment of *mon* embryos from the onset of gastrulation until 22 hpf with the CoQ analog decylubiquinone rescued *βe3 globin* expression in 26% (33/126) of *mon* embryos (Fig. 5E and fig. S21). We propose that in the absence of *tif1γ*, mitochondrial respiratory capacity is impaired because of insufficient electron transfer from complexes I and II to complex III of the ETC, thus shifting the balance in the hemogenic mesoderm to the undifferentiated cell state. Supplying *mon* embryos with CoQ boosts mitochondrial respiration and promotes erythroid differentiation.

Discussion

Tissue differentiation can be regulated by metabolic activities. It was previously unclear how lineage transcription factors induce distinct changes during cell fate specification and lineage differentiation. Our work demonstrates that the metabolic state of the tissue required for early erythroid lineage differentiation is under the direct transcriptional control of TIF1γ. CoQ is a critical downstream effector of TIF1γ transcriptional activity, regulating the balance between nucleotide synthesis and ETC activity in embryonic erythropoiesis. This highlights a previously unappreciated role of mitochondrial respiration in driving the early

commitment of the erythroid lineage. It has been proposed that transcriptional and metabolic processes influence each other (32, 33). We demonstrate that this is the case in early erythropoiesis, where exogenous CoQ can drive erythroid differentiation in the *mon* mutant, including the expression of embryonic *globin* as a late lineage marker. This study thus offers the possibility for metabolic therapeutics that could be used to target otherwise difficult-to-treat deficiencies in transcriptional programs.

Supplementary Material

Refer to Web version on PubMed Central for supplementary material.

ACKNOWLEDGMENTS

We thank R. Mori and M. C. Nonato for generating the DHODH alignment and structural model; L. Krug for excellent care of our fish; C.-Y. Chiang, E. Lee, S. Kemet, W. Chaudhry, T. Schlaeger, D. Gupta, L. Rubin, T. Arvanites, K. Nybakken, and V. Oza for technical assistance with the chemical suppressor screen; S. Freyer, J. Weiss, and H. Moreau for other technical assistance; M. Prasad for help with RNA-seq data mapping; members of the Zon laboratory for discussions; and A. B. Cantor and B. Boettner for critical reading of the manuscript.

Funding:

This work was supported by the National Heart, Lung, and Blood Institute (grants 4R01HL048801, 5P01HL032262, 5U01HL134812, and 1P01HL131477 to L.I.Z.); the National Institute of Diabetes and Digestive and Kidney Diseases (grants 1U54DK110805 and 3R24DK092760 to L.I.Z.); Harvard Catalyst (L.I.Z.); the Canadian Institutes of Health Research (foundation grant FDN0159916 to S.H. and Y.W.); the National Cancer Institute (grant 5R01CA213062 to M.C.H.); the National Institute of General Medical Sciences (grant R35GM127045 to S.L.S.); the National Human Genome Research Institute (grant U54-HG008097 to M.P.); the Cancer Research Institute (I.E.); and the American Lebanese Syrian Associated Charities (B.J.A.).

REFERENCES AND NOTES

1. Baron MH, Stem Cells 31, 849–856 (2013). [PubMed: 23361843]
2. Palis J, Front. Physiol 5, 3 (2014). [PubMed: 24478716]
3. Lensch MW, Daley GQ, Curr. Top. Dev. Biol 60, 127–196 (2004). [PubMed: 15094298]
4. Orkin SH, Zon LI, Cell 132, 631–644 (2008). [PubMed: 18295580]
5. Cabezas-Wallscheid N et al., Cell 169, 807–823.e19 (2017). [PubMed: 28479188]
6. Aucagne R et al., J. Clin. Invest 121, 2361–2370 (2011). [PubMed: 21537084]
7. Bai X et al., Dev. Biol 373, 422–430 (2013). [PubMed: 23159334]
8. He W et al., Cell 125, 929–941 (2006). [PubMed: 16751102]
9. Ransom DG et al., PLOS Biol. 2, E237 (2004). [PubMed: 15314655]
10. Ransom DG et al., Development 123, 311–319 (1996). [PubMed: 9007251]
11. Bai X et al., Cell 142, 133–143 (2010). [PubMed: 20603019]
12. Lieberman I, Kornberg A, Biochim. Biophys. Acta 12, 223–234 (1953). [PubMed: 13115431]
13. Williamson RA et al., J. Biol. Chem 270, 22467–22472 (1995). [PubMed: 7673235]
14. O'Donnell EF et al., PLOS ONE 5, e13128 (2010). [PubMed: 20957046]
15. Liu S, Neidhardt EA, Grossman TH, Ocain T, Clardy J, Structure 8, 25–33 (2000). [PubMed: 10673429]
16. Carvalho L, Heisenberg CP, Trends Cell Biol. 20, 586–592 (2010). [PubMed: 20674361]
17. Donovan A et al., Nature 403, 776–781 (2000). [PubMed: 10693807]
18. Chen JJ, Jones ME, Arch. Biochem. Biophys 176, 82–90 (1976). [PubMed: 184741]
19. Pagliarini DJ et al., Cell 134, 112–123 (2008). [PubMed: 18614015]
20. Fischer M, Oncogene 36, 3943–3956 (2017). [PubMed: 28288132]
21. Martínez-Reyes I, Chandel NS, Nat. Commun 11, 102 (2020). [PubMed: 31900386]

22. Ansó E et al., Nat. Cell Biol 19, 614–625 (2017). [PubMed: 28504706]
23. Weinberg SE et al., Nature 565, 495–499 (2019). [PubMed: 30626970]
24. Gusic M et al., Am. J. Hum. Genet 106, 102–111 (2020). [PubMed: 31883641]
25. Islam MS, Leissing TM, Chowdhury R, Hopkinson RJ, Schofield CJ, Annu. Rev. Biochem 87, 585–620 (2018). [PubMed: 29494239]
26. Stachura DL, Chou ST, Weiss MJ, Blood 107, 87–97 (2006). [PubMed: 16144799]
27. Madak JT, Bankhead A 3rd, Cuthbertson CR, Showalter HD, Neamati N, Pharmacol. Ther 195, 111–131 (2019). [PubMed: 30347213]
28. Wang Y, Hekimi S, Trends Cell Biol. 26, 367–378 (2016). [PubMed: 26827090]
29. Stefely JA, Pagliarini DJ, Trends Biochem. Sci 42, 824–843 (2017). [PubMed: 28927698]
30. Mollet J et al., J. Clin. Invest 117, 765–772 (2007). [PubMed: 17332895]
31. Casey AC, Bliznakov EG, Cancer Res. 33, 1183–1186 (1973). [PubMed: 4718669]
32. Donati S, Sander T, Link H, Wiley Interdiscip. Rev. Syst. Biol. Med 10, e1396 (2018).
33. Guijas C, Montenegro-Burke JR, Warth B, Spilker ME, Siuzdak G, Nat. Biotechnol 36, 316–320 (2018). [PubMed: 29621222]

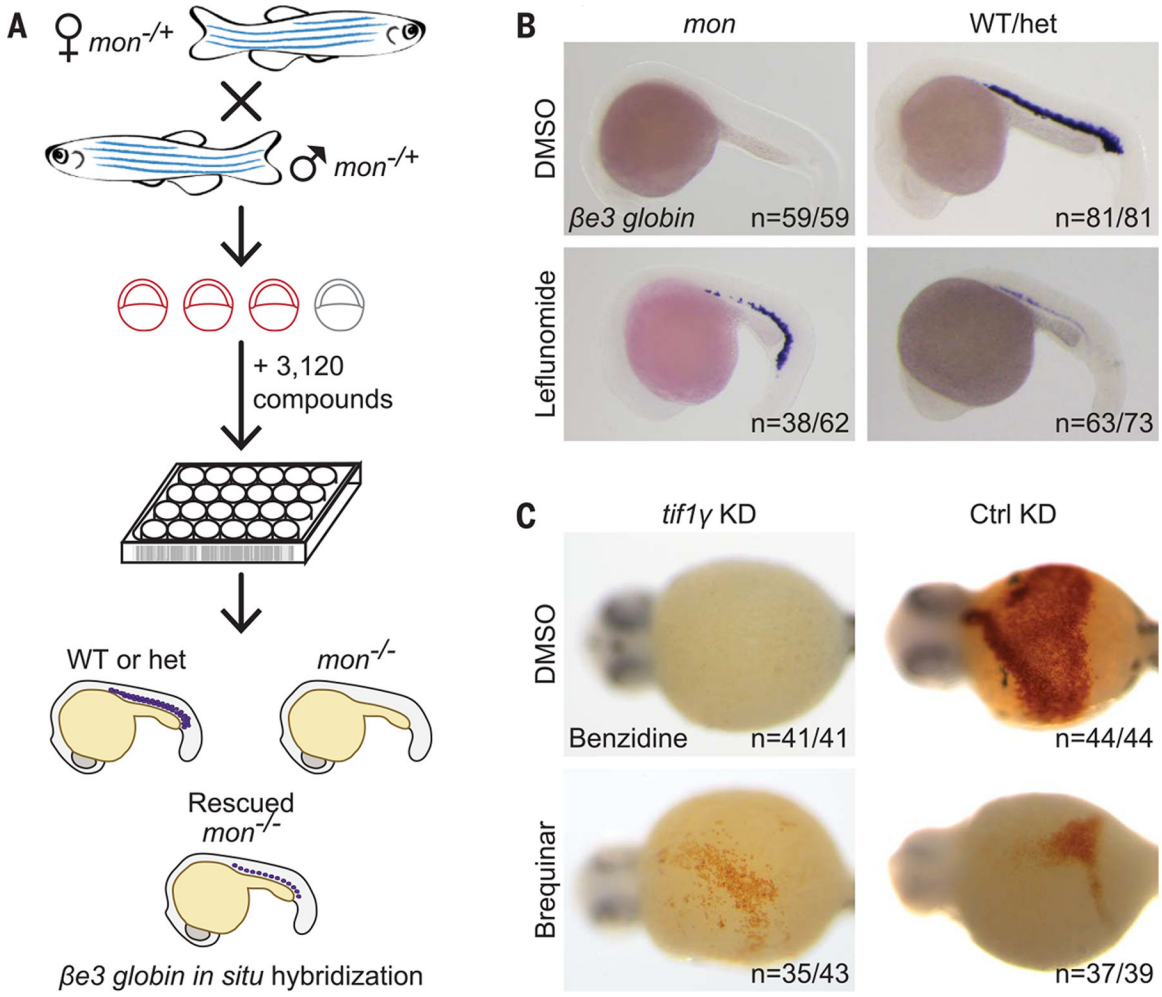

Fig. 1. Chemical suppressor screen for the *mon* zebrafish mutant identifies DHODH inhibitors to rescue primitive erythropoiesis.

(**A**) Cartoon depicting chemical screening strategy. WT, wild type; het, *mon* heterozygous. (**B**) WISH for *βe3 globin* in *mon* and WT or het zebrafish embryos at 22 hpf treated with 7 μM leflunomide or DMSO. *N* (number of biological replicates) = 4. Cumulative results are shown. (**C**) Benzidine staining of embryos at 44 hpf after morpholino-mediated knockdown of *tif1γ* (*tif1γ* KD) or standard control knockdown (Ctrl KD) and treatment with 3.5 μM brequinar or DMSO from 5.3 hpf until 11.7 hpf. *N* = 3. Data from one representative experiment are shown. n = number of embryos with depicted phenotype/number of all embryos tested (see also fig. S1).

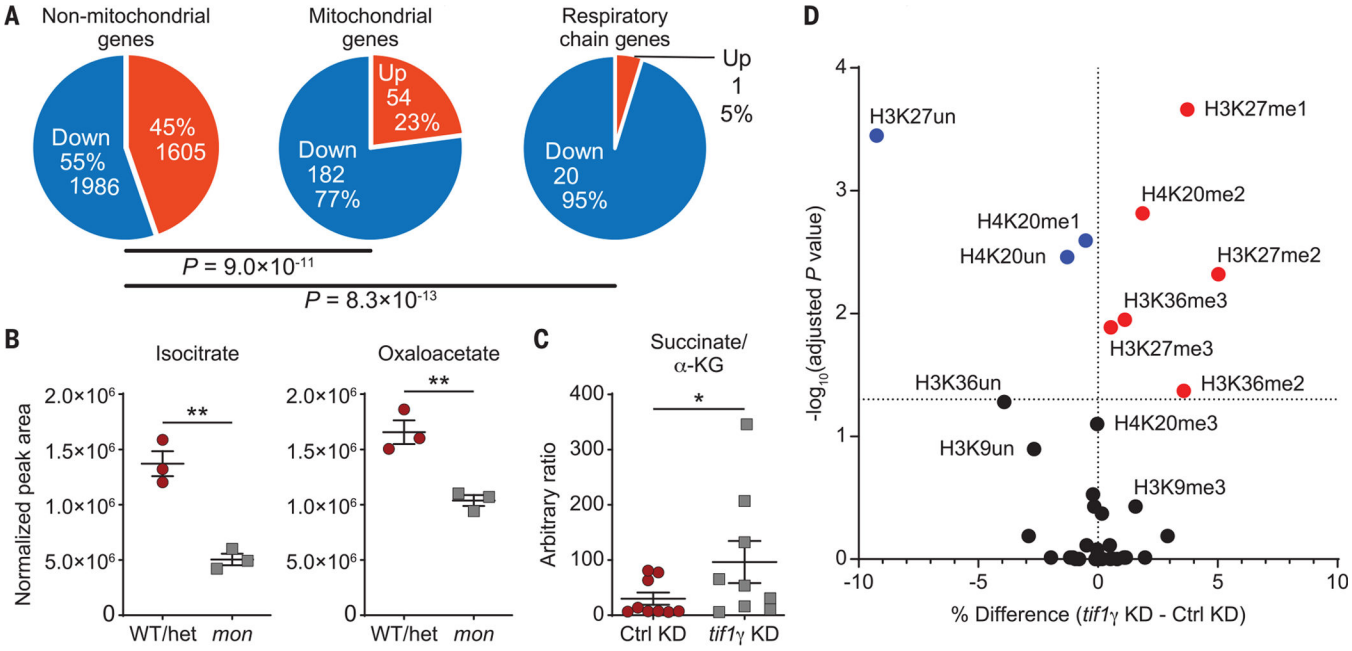

Fig. 2. *tif1γ* loss affects the TCA cycle and histone methylation.

(**A**) RNA-seq data at 10 hpf showing all up- or down-regulated [FPKM (fragments per kilobase of transcript per million mapped reads) >1, $q < 0.05$] nonmitochondrial (left), mitochondrial (middle), and respiratory chain genes (right) in *tif1γ* KD or Ctrl KD embryos treated with DMSO from 5.3 hpf until 10 hpf. *P* values were determined by Pearson's chi-squared test with default parameters. (**B**) Levels of the indicated TCA cycle metabolites in *mon;Tg(drl:EGFP)* or sibling WT or het embryos at 22 hpf as measured by untargeted metabolomics. $N = 3$. Normalization by median correction. Data are shown as means ± SEM by two-tailed *t* test. (**C**) Succinate/α-KG ratio in *tif1γ* KD or Ctrl KD embryos at 22 hpf as measured by untargeted metabolomics. Data are shown as means ± SEM by two-tailed *t* test. (**D**) Volcano plot of percentage occupancy data of histone posttranslational modifications (PTMs) in *tif1γ* KD compared with Ctrl KD embryos at 22 hpf. Each dot represents a single modification at the amino acid level. *x*-axis shows the percentage difference between the means of *tif1γ* KD and Ctrl KD samples. Adjusted *P* values were determined by multiple *t* tests between all five replicates across the two conditions. Significantly enriched histone PTMs in *tif1γ* KD and Ctrl KD samples are shown in red and blue, respectively. $^{**}P < 0.01$; $^{*}P < 0.05$; ns, not significant (see also figs. S5 to S12).

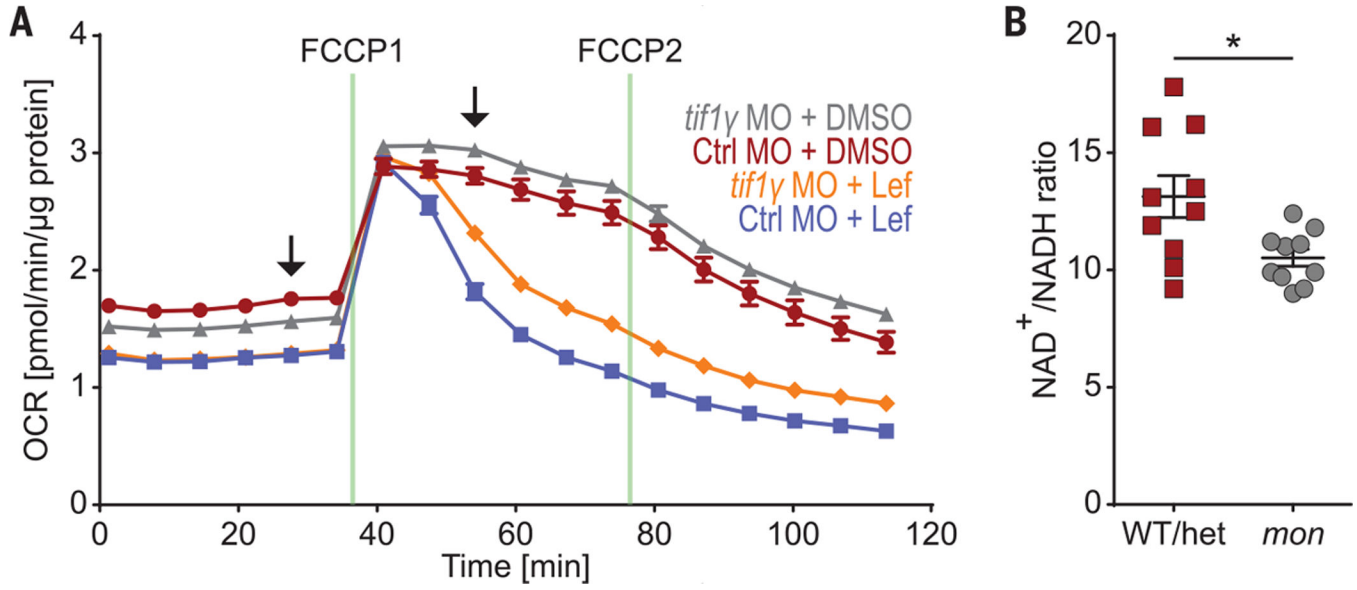

Fig. 3. *tif1γ* loss leads to a functional mitochondrial defect.

(**A**) OCR as measured by Seahorse analysis of single *tif1γ* KD or Ctrl KD embryos at 16 hpf treated with 7 µM leflunomide or DMSO from 5.3 until 11 hpf. $N = 3$. Data from one representative experiment are shown. Data are shown as means ± SEM. Arrows indicate time points for which statistical analysis is shown in fig. S14, A and B. (**B**) Analysis of NAD^+/NADH ratio in *mon* and sibling WT or het embryos at 48 hpf using the NAD/NADH-Glo Assay. $N = 3$. Cumulative results are shown. One data point indicates one embryo. $^*P < 0.05$, two-tailed *t* test.

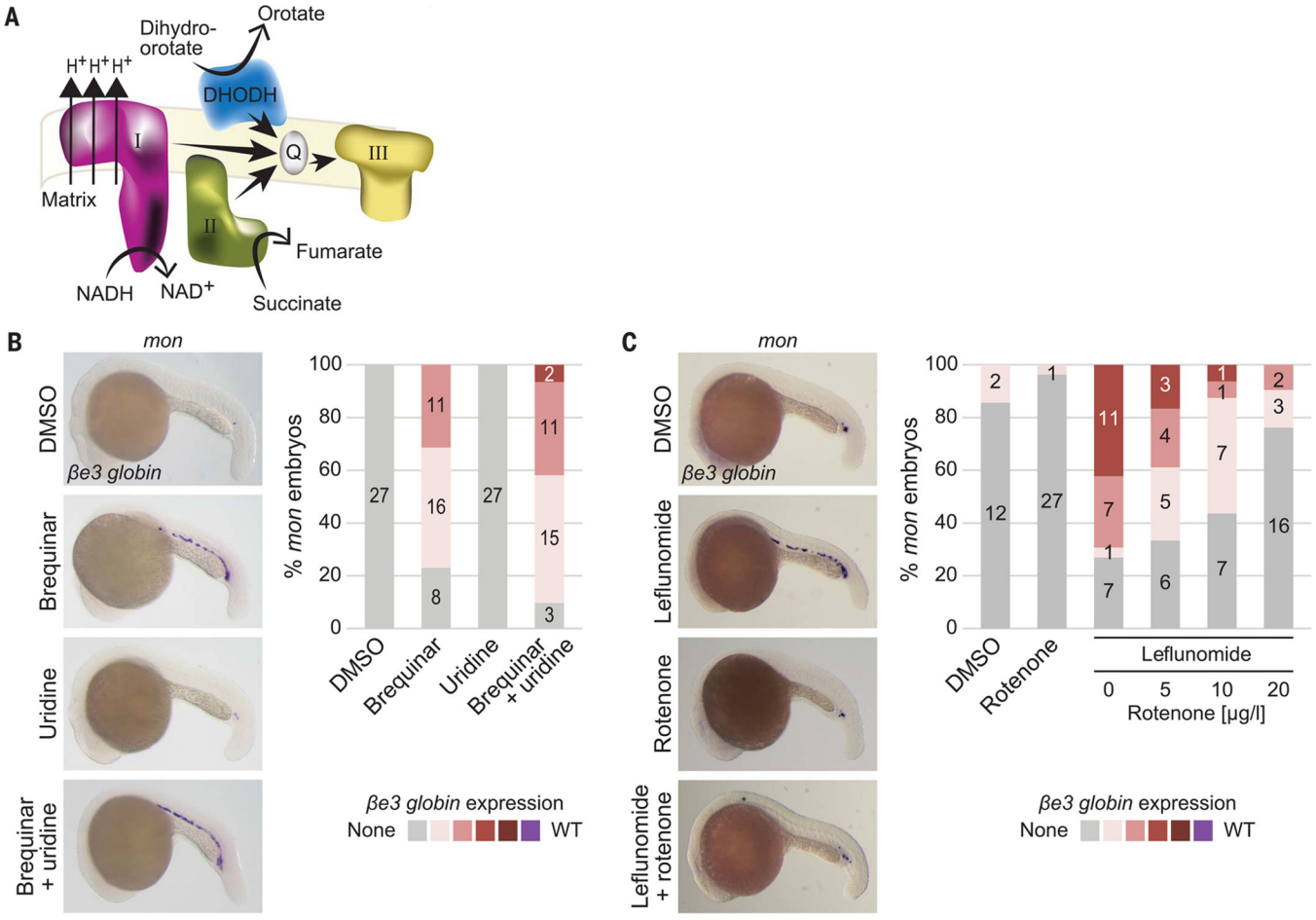

Fig. 4. Function of *tif1γ* in erythropoiesis is linked to the ETC.

(**A**) Cartoon depicting relationship of DHODH with some components of the mitochondrial ETC. (**B** and **C**) Representative *βe3 globin* WISH images (left) and quantification (right) of *mon* embryos at 22 hpf treated with DMSO or 3.5 μM brequinar alone or in combination with 100 mM uridine [(B); $N = 4$] or treated with DMSO or 7 μM leflunomide alone or in combination with 5, 10, or 20 μg/L rotenone [(C); $N = 3$]. Cumulative results are shown. Numbers in columns in (B) and (C) refer to the number of embryos with the color-coded degree of *βe3 globin* staining (see also fig. S15).

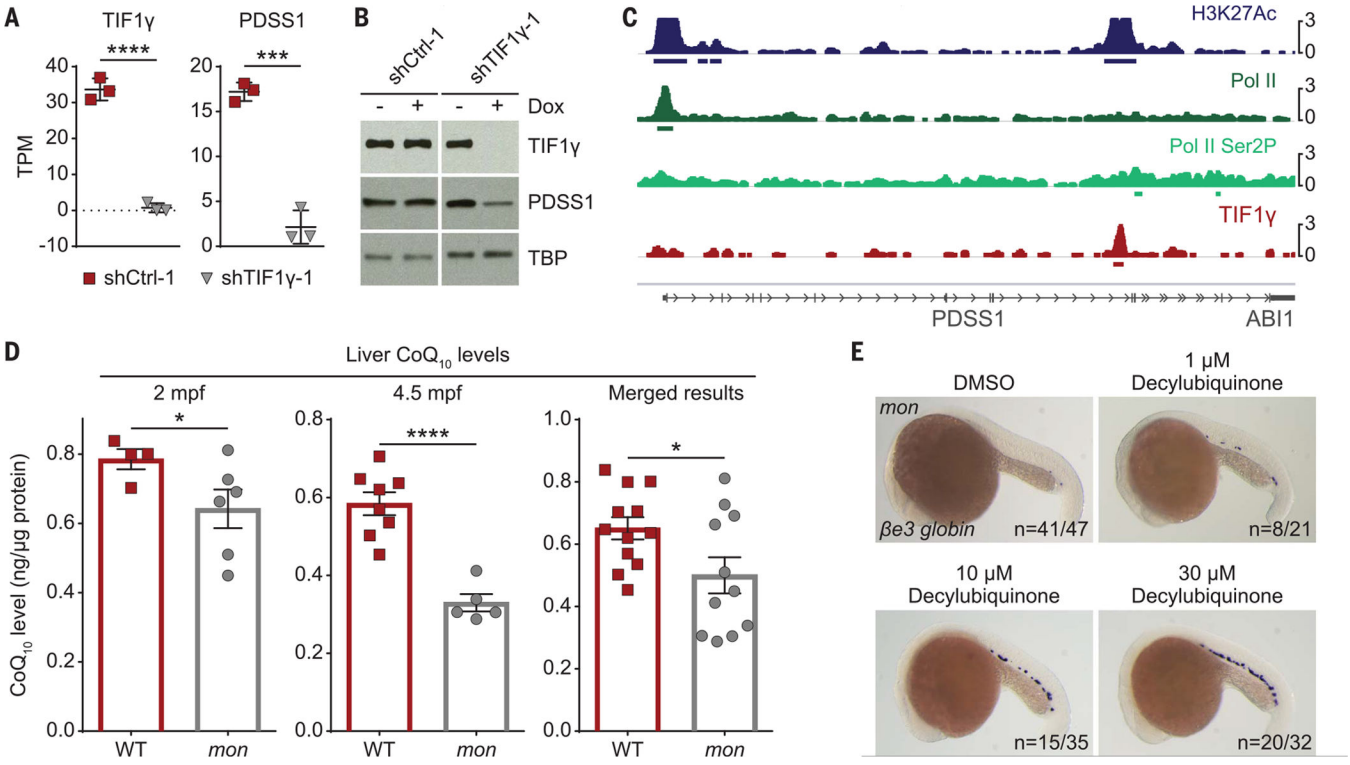

Fig. 5. CoQ is a functional target of *tif1γ* in primitive erythropoiesis.

(**A**) RNA-seq data showing transcripts per kilobase million (TPM) of *TIF1γ* and *PDSS1* in two stable HepG2 clones carrying either an inducible shRNA targeting *TIF1γ* (shTIF1γ-1) or a control shRNA (shCtrl-1) 48 hours after induction with doxycycline. $N = 3$. Results were analyzed with two-tailed *t* test. (**B**) Western blot of TIF1γ and PDSS1 for the experiment described in (A). TBP was used as the loading control. (**C**) IGV output of a 52-kb genomic region around *PDSS1* on chromosome 10 showing the chromatin occupancy by ChIP-seq for H3K27Ac, Pol II, Pol II phosphorylated at serine 2 (Pol II Ser2P), and TIF1γ in HepG2 cells. (**D**) CoQ_{10} quantification of adult *mon* and WT livers at indicated time points by HPLC. mpf, months postfertilization. Merged results are shown on the right. Each dot represents five pooled livers (except for one sample per genotype at 4.5 mpf, which only contained three livers). Normalization to total protein amount per sample. (**E**) Representative *βe3 globin* WISH images of embryos at 22 hpf treated with DMSO or 1, 10, 20, or 30 µM decylubiquinone. $N = 3$. Cumulative results are shown. ****$P < 0.0001$; ***$P < 0.001$; *$P < 0.05$ (see also figs. S18 to S21).